Quaternary Science Reviews 28 (2009) 2600–2615

Contents lists available at ScienceDirect

Quaternary Science Reviews

journal homepage: www.elsevier.com/locate/quascirev

A late Pleistocene record of aeolian sedimentation in Blanche Cave, Naracoorte, South Australia

Nicolas Darrénougué [a], Patrick De Deckker [a,*], Kathryn E. Fitzsimmons [a], Marc D. Norman [a], Liz Reed [b], Sander van der Kaars [c], Stewart Fallon [a]

[a] Research School of Earth Sciences, The Australian National University, Canberra ACT 0200, Australia
[b] School of Biological Sciences, The Flinders University of South Australia, GPO Box 2100, Adelaide SA, 5001, Australia
[c] Centre for Palynology and Palaeoecology, School of Geography and Environmental Science, Monash University, Vic. 3800, Australia

ARTICLE INFO

Article history:
Received 19 December 2008
Received in revised form
18 May 2009
Accepted 22 May 2009

ABSTRACT

We provide geochemical analyses and grain size data for a clearly layered, 80 cm thick sedimentary deposit close to a roof collapse in Blanche Cave near Naracoorte in SE South Australia. This deposit contains aeolian material deposited between ~40 ka and 14 ka cal BP and which yields airborne sediments spanning the Last Glacial Maximum, a period of time with little information for the Australian continent. The deposit also contains abundant vertebrate fossil material derived from owl pellets, accumulation and pitfall entrapment. Below the studied profile, large vertebrate remains are found but are not discussed here. No Holocene sedimentation occurred at the site examined in the cave, and the top of the sequence is capped with a layer that has been anthropologically disturbed and contains exotic *Pinus* pollen. Chronologies of the deposit were obtained using two dating techniques: single stage accelerator mass spectrometer (SSAMS) ^{14}C analysis of 23 charcoal samples and optically stimulated luminescence (OSL) dating of quartz from 6 sediment samples. The ^{14}C chronology is preferred to describe the history of the deposits since the OSL chronology, which consistently overestimates the associated radiocarbon dates, may be inaccurate due to complexities in calculating dose rates, and may in addition represent the timing of sediment deposition through the cave opening rather than sediment transport to the deposit site. Morphological analysis of single quartz grains and grain size analysis indicate different provenance that is confirmed through the geochemical analyses of bulk sediment. Major elements were measured by X-ray Fluorescence (XRF), trace and rare earth elements by Laser Ablation Inductively Coupled Plasma Mass Spectrometry (LA ICP-MS), and Neodymium isotopic ratios were obtained using a Thermal Ionisation Mass Spectrometer (TIMS).

Our results indicate that the aeolian material deposited in Blanche Cave over the 40–14 ka cal BP period originated from different sources across South Australia, although Nd isotopes clearly indicate a close association with sediments of the Kanmantoo Group outcropping along the eastern portion of the Mount Lofty Ranges and the Padthaway Ridge further south, both being located to the NW and NNW of the cave. During the latter part of Marine Isotope Stage 3, conditions were wetter and windblown sediment came from the coastal region just north and south of the Coorong Lagoon, with winds originating from the north-northwest. At that time, woody taxa appear to have vegetated the landscape. During the drier phases, especially the Last Glacial Maximum, sediment came from further inland, thus suggesting a different predominant wind direction, more from the northwest. The deglaciation saw material originating from a more northerly direction.

1. Introduction

Located in the south-eastern part of the state of South Australia, the Naracoorte Caves National Park was inscribed on to the World Heritage list in 1994 for its outstanding Quaternary vertebrate fossil deposits. These deposits span the past 500,000 years,

* Corresponding author. Tel.: +612 6125 2070; fax: +612 6125 5544.
E-mail address: patrick.dedeckker@anu.edu.au (P. De Deckker).

0277-3791/$ – see front matter © 2009 Elsevier Ltd. All rights reserved.
doi:10.1016/j.quascirev.2009.05.021

providing the most complete record of Quaternary vertebrates in Australia at one locality (Reed and Bourne, 2000). The aim of palaeontological research at the caves is to track faunal and environmental change over time. The cave system is situated in the uplifted portion of a phreatic karst in the Tertiary Gambier Limestone that underlies the southeast of South Australia. Cave development occurred during the early to mid-Pleistocene. The study site for this paper is Blanche Cave, one of 26 caves within the Naracoorte Caves National Park, 12 km southeast of the Naracoorte township. It was discovered by early settlers in 1845 and was the first site to receive palaeontological attention at Naracoorte when the Reverend Julian Tenison Woods visited in 1857 (Reed and Bourne, 2000).

Blanche Cave consists of three chambers, which can be accessed via three large roof collapse windows (Fig. 1). The collapse of some parts of the cave roof must have occurred during the late Quaternary, leading to the accumulation of Pleistocene and Holocene sediments and vertebrate remains in the vicinity of the collapse windows. Sediment deposits within the caves are typically deep and well stratified, derived from the surrounding surface soils and aeolian material. The sediments found within the caves are similar to those found locally in the Naracoorte region, and it has been proposed that the cave sediments were locally derived (Forbes et al., 2007). Characteristic local sediments include the famous Terra Rossa soils of the Coonawarra and Naracoorte region, also called Red Brown Earths (RBEs). These formed as a pedogenic mantle over the Gambier Limestone during the Quaternary, and consist of a sandy A horizon and a red clay B horizon (Mee et al., 2004). Sediments derived from the Terra Rossa soils are thought to have formed part of cave fills since the mid-Pleistocene (Wells et al., 1984). In addition, quartz-and clay-rich sediments derived from the Murray River deposits are also thought to have contributed to the cave deposits, transported by the northwest prevailing wind regime (Forbes and Bestland, 2007).

The presence of cave sediment sequences exceeding 500 ka (Moriarty et al., 2000; Prideaux et al., 2007) indicates that some caves at Naracoorte (Victoria Fossil Cave and Cathedral Cave) opened during the early middle Pleistocene. Other caves, notably Robertson, Blanche and Wet Caves, contain much younger, late Pleistocene to Holocene material (Forbes and Bestland, 2006, 2007) which suggests that these caves opened more recently. The Blanche Cave deposits span at least the last 40,000 years based on U/Th chronology of calcareous straws that fell from the roof of the cave and became incorporated into the deposit studied here (St Pierre et al., 2009). Sedimentological analysis of the younger Naracoorte sequences provides important local palaeoenvironmental and palaeomorphological information, potentially more continuous and at a higher resolution than is provided by the surrounding soils deposits (e.g. the Terra Rossa soils studied by Mee et al., 2004).

A palaeontological excavation of a sediment deposit in the third chamber has been undertaken by one of the authors (LR) and T. Laslett (Laslett, 2006). To date, the site has yielded 68 species of amphibians, reptiles, birds and mammals. Taphonomic analysis has revealed that vertebrate remains accumulated via multiple accumulating modes, notably owl pellet deposition, pitfall entrapment

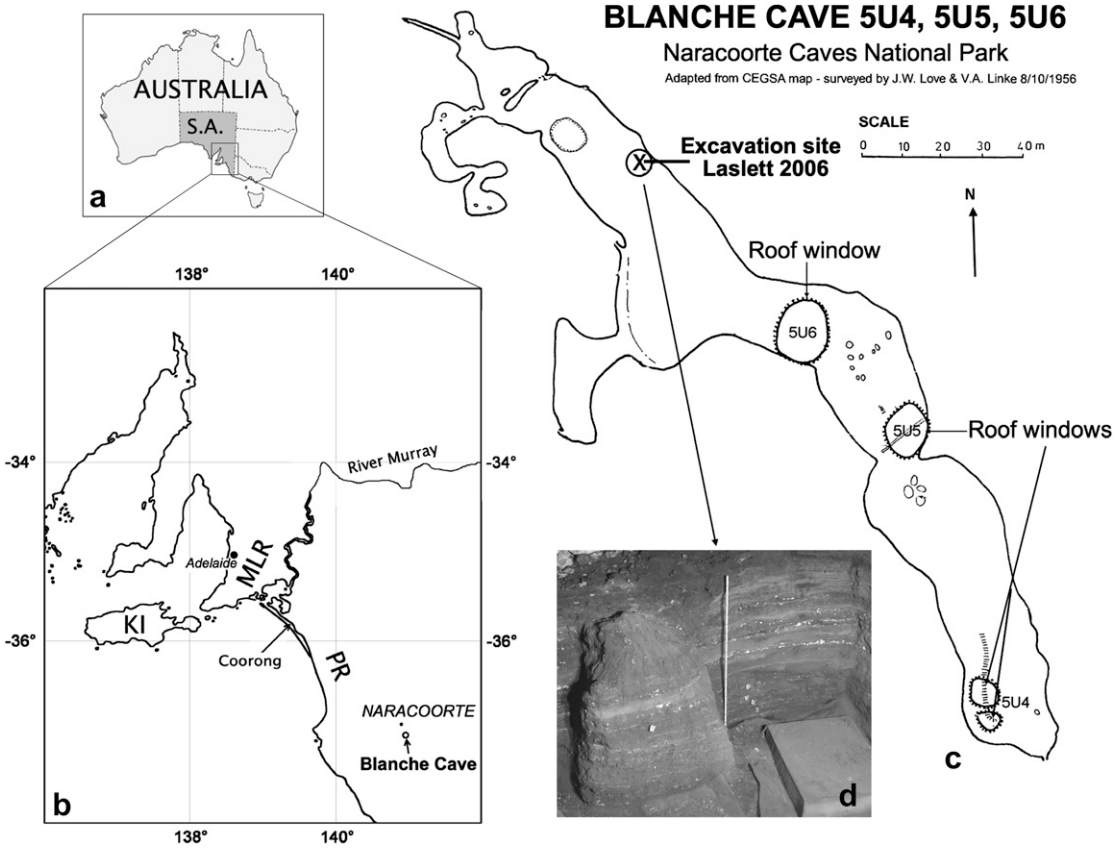

Fig. 1. Location of Blanche Cave showing: a. a map of Australia and South Australia; b. the southeastern region of South Australia showing Naracoorte and the main surrounding geological formations (KI: Kangaroo Island; MLR: Mount Lofty Ranges; PR: Padthaway Ridge); c. a map of Blanche Cave with the site where the core was taken; d. a photo of the pit dug after the core was taken. Note the fine layering and the presence of cave straws which must have fallen from the cave roof. The straws occur at very specific levels [see text for more information].

and natural deaths of cave dwelling species. The site is well stratified with the potential for high resolution palaeoecological analysis of biodiversity change over time during the late Quaternary. Critical to this is a chronological and environmental context for the vertebrate remains.

This study provides a high-resolution geochemical, sedimentological and geochronological analysis of the sedimentary sequence at Blanche Cave, providing important palaeoenvironmental and chronological context for the vertebrate fossil deposit. Geochemical fingerprinting identifies the origin of the cave sediments using the combined techniques of X-Ray Fluorescence (XRF), Laser Ablation ICP Mass Spectrometry (LA ICP-MS) and Thermal Ionisation Mass Spectrometry (TIMS). The pollen record of the sequence is also investigated here. The sequence is chronologically constrained using the independent dating techniques of optically stimulated luminescence (OSL) of quartz sand and radiocarbon dating of charcoal particles. The palaeoenvironmental reconstruction provides new insight into the relatively cold, arid period of the LGM for inland Australia for which there are relatively few continuous records.

2. Materials and methods

2.1. The core

The palaeoenvironmental record is derived from a core taken during a palaeontological excavation in the third chamber of Blanche Cave in January 2007. Since the cave deposits are typically unconsolidated, a 15 cm wide PVC tube of 100 cm length was driven into the sediment to a depth of 80 cm. Until the core was opened in the laboratory, the tube was kept vertical in a cold room to prevent chemical alteration and minimise mixing.

Fig. 2 summarises the sediments and stratigraphy. Sediment colour was described using the Revised Standard Soil Colour Charts. A total of 58 samples were taken for sedimentological analysis from 34 identified units. Within the thicker units, samples were taken at 1.5 cm intervals.

2.2. Morphological analysis

2.2.1. Grain roundness

Each sample was observed using an optical microscope with 50 times magnification. This permitted an estimation of mean grain size, level of roundness and possible coating of quartz grains.

2.2.2. Grain size analysis

Prior to grain size analysis, samples were immersed in 38% HCl for a few minutes to dissolve all the carbonates. The liquid containing the residual fraction was then centrifuged twice to remove the organic-matter fraction (e.g. charcoal component). Through this process, only the silicate fraction was recovered.

Grain size analysis of the silicate fraction of 57 samples was carried out at the University of Bordeaux I using a Mastersizer S laser diffraction microgranulometer using the Franof method with a polydispersive analysis model following the methods of Pichevin et al. (2005). Grain size results came out as a grid of 64 size classes ranging from 0.06 μm up to 878.67 μm diameter.

2.2.3. Scanning electron microscopic observations

Scanning Electron Microscope (SEM) analysis was performed on quartz grains from 16 representative samples along the core. Prior to examination under the SEM, the individual grains were stuck on non conductive, double-sided sticky tape and then coated with a very thin layer of gold.

2.3. Dating of the core

2.3.1. Radiocarbon dating

Charcoal was collected by hand from the depth profile using a trowel that was cleaned between each sample. The samples were immediately placed in aluminium foil and placed in individual bags. In the laboratory, the sediment was removed from the charcoal and samples weighing 5–7 mg were pre-treated using the acid-alkali-acid standard pre-treatment (1 M HCl, 1 M NaOH, 1 M HCl). Samples were then rinsed in 18 MΩ water until a neutral pH was obtained (usually 3–5 rinses). Samples weighing 2.5–3 mg were then loaded in quartz tubes with CuO and silver wire. These were sealed under vacuum and baked at 900 °C to convert the sample into carbon dioxide. The CO_2 was then converted to graphite by hydrogen reduction in the presence of iron powder at a temperature of 550 °C. The sample was placed in a small holder and pressed into a small pellet and was run on the Australian National University Single Stage Accelerator Mass Spectrometer (SSAMS). A sample wheel contains 39 samples, 6 are the primary radiocarbon standard Oxalic Acid I, 4 are secondary standards/known age material and 2 are carbon-14 free material, in this study this is USGS coal. Measurements of known age material are within 3‰ of their accepted ages, and results from the TIRI-K (turbidite) sample averages ($n = 25$) 18, 140 ± 40 (accepted 18,155) (Fallon et al., in press). The results are corrected for their $\delta^{13}C$ and the quoted age is in radiocarbon years using the Libby half life of 5568 years and following the conventions of Stuiver and Polach (1977). Table 1 shows the results which are given in percent modern carbon (pMC), conventional radiocarbon age and calendar age. The conventional radiocarbon ages were calibrated to a calendar age using Calib 5.0 (Stuiver and Reimer, 1993; Reimer et al., 2004) and the Bard polynomial for radiocarbon ages >25,000 yr (Bard, 1998). Sample preparation backgrounds have been subtracted using measurements of ^{14}C free coal and wood.

2.3.2. OSL dating

Six samples were taken from sandy units within the core for OSL dating. The samples were collected from the core under low intensity red light. The top 2 cm of sediment on the surface of the core section was removed to ensure that the OSL sample had not been exposed to light during earlier sampling of the core. The underlying material from the selected sandy intervals was collected in vials for processing.

Sand-sized quartz was isolated from other minerals by dilute hydrochloric acid (HCl) digestion to remove carbonates (e.g. Huntley et al., 1993), followed by oxidation in hydrogen peroxide to remove organic components. Grains were then etched in 40% solution of hydrofluoric acid for 100 min to remove feldspars and the outer rinds of quartz exposed to alpha radiation, rinsed in HCl and dried. The resulting clean quartz grains were then sieved to isolate the modal grain size of 125–180 μm, which were mounted onto the central 1 of 10 mm diameter stainless-steel discs using silicone oil. Aliquots of this size contain fewer than 50 grains (Duller, 2008). Considering rarely more than a few percent of grains yield a measurable luminescence signal (e.g. Jacobs et al., 2006; Porat et al., 2006), these small aliquots were considered to effectively yield the same information as single grain dating with respect to bleaching of the sediments at deposition (Olley et al., 1998; Rhodes, 2007).

Equivalent dose (D_e) measurements were undertaken using a Risø TL-DA-12 reader, with light stimulation provided by blue light-emitting diodes (Botter-Jensen et al., 1999, 2000). The luminescence signal arising from the quartz was detected by an EMI 9325QA photomultiplier tube with a coated Hoya U-340 filter (Botter-Jensen, 1997). Sample irradiation was provided by a 90Sr/90Y beta source (Botter-Jensen et al., 2000). De was measured for 24 small aliquots of each sample using the single-aliquot regenerative-dose protocol

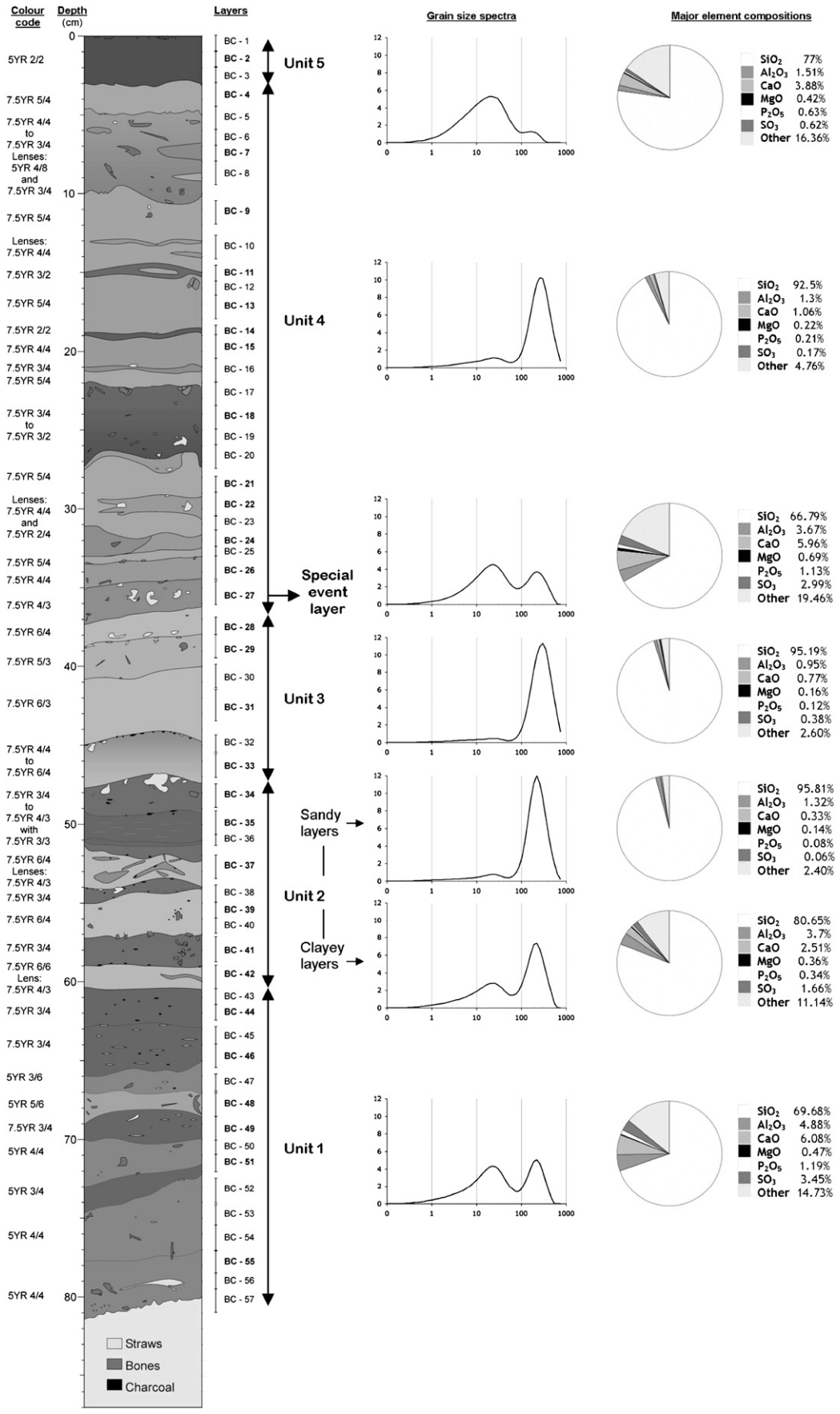

Fig. 2. Stratigraphic log of the core from Blanche Cave. On the left are the colour codes using the modified Munsell Chart. On the right hand side of the diagram are the positions of all samples analysed from the core. The core is divided into 5 separate units and grain size spectra representative of each unit are displayed. Next to these are the major element analyses done by XRF.

(SAR) of Murray and Wintle (2000), with an infrared (IR) bleach prior to OSL signal measurement to identify potential feldspar contamination of the quartz. Sample De were calculated using the central age model of Galbraith et al. (1999).

Dose rates were calculated using *in situ* gamma spectrometry for the gamma component, and inductively coupled plasma (ICP) analysis for the beta component. *In situ* gamma spectrometry was measured using a 1.5 inch sodium iodide detector from the pit face adjacent to where the core was taken, at equivalent stratigraphic positions to the samples. Gamma spectrometry was unable to be undertaken for the shallowest sample (K2014a) due to the friability of the sediment. For this sample, the gamma contribution to dose rate was calculated by deriving the relative contribution of the three topmost units in the core to that sample's depth based on formulae published in Aitken et al. (1985), and using the ICP-MS concentrations of K, Th and U for those units. This method of calculation was also used to compare the gamma dose rates derived from ICP-MS results with *in situ* gamma spectrometry for the other samples, and the two sets of dose rate values were found to be within 10% difference of one another. Gamma ray contribution from the surrounding cave wall and roof limestone was assumed to be negligible relative to that of the cave floor sediment.

ICP mass spectrometry was used to measure uranium, thorium and potassium content (see Section 2.4), which was used to calculate the beta component of the dose rate. *In situ* moisture content for beta dose attenuation was determined by weighing the raw and oven-dried weight of sediment samples representing the OSL sample depths, with added uncertainties to allow for likely variations in moisture content based on sediment porosity. Calculations for the cosmic ray contribution to dose rate took into account the surveyed thickness of the cave roof and were based on the formulae of Prescott and Hutton (1994).

2.4. Geochemical determination of major elements, trace elements and isotopic ratios

2.4.1. Major elements geochemistry by XRF

X-Ray Fluorescence analysis (XRF) was performed on 30 bulk samples from the core in order to determine the percentage composition of major elements in their oxidised state (SiO_2, Al_2O_3, CaO, MnO, MgO, Na_2O, K_2O, TiO_2, P_2O_5, SO_3 and Fe_2O_3 – note this is total Fe reported as Fe_2O_3). Samples were prepared by crushing with an agate mortar and pestle with ethanol into a very fine powder. After an overnight dry at 40 °C, 0.2700 g ± 0.0030 of each sample was weighed and mixed with 1.7200 g ± 0.0030 of a 12:22 ithium tetraborate and lithium metaborate flux in Pt–Au crucibles. Half a millilitre of 20% $LiNO_3$ solution was added to oxidise any sulphur present. The crucibles were placed into a 400 °C furnace to dry and the mixture was fused in fused a 1080 °C rocker furnace, with an addition of NH_4I pellets to provide some 'wetting'. With the melted material, XRF disks were prepared from the molten material for analysis using graphite moulds where the fused mixture was allowed to cool, thus making glass disks.

The measurements of the 30 most representative samples were carried out in the former Department of Earth and Marine Science [now RSES] at the Australian National University (ANU) using a Phillips (PANalytical) PW2400 Wavelength Dispersive XRF Spectrometer. Results for Si, Al, Ca, Mn, Mg, Na, K, Ti, P, S, Fe, F and Cl were originally presented in percentage of their oxidised state.

2.4.2. Trace elements and rare earths by LA ICP-MS

Sample preparation for the Laser Ablation Inductively Coupled Plasma Mass Spectrometer (LA ICP-MS) follows the same protocol as the one for the making of the XRF glass disks except for the relative proportions of sample and flux. For the LA ICP-MS, disks we weighed 0.5000 g ± 0.0050 of sample mixed with 1.500 g ± 0.0050 of flux. Three batches of 10 disks were immersed in epoxy and the resin blocks containing the disks were cut to correct dimensions to fit the LA ICP-MS sample stage. Finally, the samples were polished using a diamond paste.

The trace element analyses were carried out at the Research School of Earth Science (RSES) at ANU using a pulsed excimer laser associated with an Agilent 7500 Series quadrupole ICP mass spectrometer. The laser was operated at a spot diameter of 86 μm; 10 Hz repetition rate, and 126 mJ. 30 s of background was collected on the carrier gas prior to each analysis, followed by 90 s of ablation along a 1.5 mm traverse. Data were collected using a 20 ms/mass dwell time. The NIST 612 glass was used as an external standard to calibrate the sensitivity of the elements at a rate of 2 standard analysis every 16 samples. Each analysis was normalized to the CaO wt% content of the sample (measured by XRF) to correct for variable ablation yield. Concentrations of Be, Cr, Mn, Co, Ni, Ga, Rb, Sr, Y, Zr, Nb, Sb, Cs, Ba, La, Ce, Pr, Nd, Sm, Eu, Tb, Gd, Dy, Ho, Er, Yb, Lu, Hf, Ta, Th, U were calculated using the 'Lamtrace' software developed by S.E. Jackson and discussed in Coedo et al. (2005).

2.4.3. Nd isotope ratios by TIMS

The determination of neodymium (Nd) isotope ratio was carried out at RSES, ANU using a Finnigan MAT-261 thermal ionisation mass spectrometer (TIMS) on 13 of the most representative samples of the core. A 0.10 g portion of each sample, previously crushed into a fine powder, was weighed into screw-cap teflon vials with the addition of a few drops of 2% ultrapure HNO_3 to stabilise the powder. Dissolution of the silicate content of the samples was carried out by refluxing the samples in 1 ml of HNO_3 conc. and 1 ml of HF. This protocol was repeated twice, followed by drying of the sample on a hotplate. For the third time, 1 ml of concentrated HNO_3 was added and the samples were again dried on the hotplate. Organic matter was removed from the sample using Eichrome pre-filter resin, and a REE cut was isolated from the sample matrix using Eichrome TRU-spec ion-specific resin. Samples were loaded onto the resins in 2 M HNO_3, and the REE were collected using 3 M HCl. After drying on a hotplate the samples were brought up in 0.2 N HCl and loaded onto HDEHP ion-exchange columns for purification of the Nd. For isotopic analysis, the Nd was loaded onto Ta (evaporation) – Re (ionisation) double filament assemblies in 1 M HNO_3 with dilute H_3PO_4, and run as a metal. Data were corrected for fractionation by normalisation to $^{146}Nd/^{144}Nd = 0.7219$. The $^{143}Nd/^{144}Nd$ data were corrected to a value of 0.511860 for the La Jolla Nd standard, and $\varepsilon Nd(0)$, the deviation from bulk silicate earth value in parts in 10,000, was calculated relative to $^{143}Nd/^{144}Nd = 0.512638$.

2.5. Pollen

From every sampled level, 5 cm^3 of sediment was processed. Twenty samples were initially treated with warm 10% Na-pyrophosphate ($Na_4P_2O_7$) and sieved over a 210 and a 7 μm mesh. Organic material retained in the 7 μm mesh was isolated from the remaining inorganic fraction using heavy liquid separation with sodium polytungstate ($Na_{46}[H_2W_{12}O_{40}].H_2O$; s.g. 2.0, 20 min at 2000 rpm). The isolated material was then treated with acetolysis (9 parts $(CH_3CO)_2O$: 1 part H_2SO_4, 10 min). The remaining residues were dehydrated with ethanol (C_2H_5OH). Slides were mounted with glycerol ($C_3H_5(OH)_3$) and sealed with paraffin.

3. Results

3.1. Core description

The core presents 34 layers, most of which are composed of sand-sized sediment. Stratigraphically, we identified 5 distinct

Table 1
Radiocarbon ages for selected samples from the Blanche Cave core.

Core level number	Depth in core (cm)	Unit number in core	Percent modern carbon (pMC)	pMC error 1σ	^{14}C age	14C age error 1σ	Calendar Age aBP (1σ) Calib 5.0
BC-2	2	5	21.18	0.15	12,470	60	14,502 ± 274
BC-4	4	4	20.57	0.19	12,700	80	15,000 ± 151
BC-4	8	4	19.34	0.17	13,200	80	15,621 ± 196
BC-9	11	4	19.26	0.16	13,230	70	15,665 ± 190
BC-11	15	4	18.84	0.22	13,410	100	15,901 ± 205
BC-13	17	4	19.09	0.14	13,300	70	15,767 ± 196
BC-15	20	4	18.81	0.17	13,420	80	15,931 ± 204
BC-18	24	4	17.75	0.16	13,890	80	16,548 ± 214
BC-24	32	4	17.12	0.14	14,160	70	16,941 ± 259
BC-24 repeat	32	4	16.93	0.17	14,270	90	17,069 ± 243
BC-27	36	4	8.28	0.11	20,010	110	23,969 ± 159
BC-28	38	3	13.89	0.17	15,860	100	19,043 ± 102
BC-29	39	3	12.94	0.13	16,430	90	19,637 ± 195
BC-33	46	3	11.82	0.14	17,160	100	20,279 ± 128
BC-34	48	2	14.72	0.16	15,390	90	18,747 ± 71
BC-35	50	2	15.08	0.16	15,200	90	18,629 ± 98
BC-39	56	2	9.94	0.13	18,550	110	22,153 ± 114
BC-41	58	2	8.29	0.12	20,000	120	23,959 ± 168
BC-42	60	2	7.70	0.12	20,590	130	24,661 ± 238
BC-44	62	1	7.59	0.12	20,710	130	24,802 ± 212
BC-46	65	1	7.63	0.12	20,670	130	24,756 ± 237
BC-48	68	1	4.38	0.12	25,120	220	29,489[a]
BC-49	69	1	3.04	0.09	28,070	230	32,820[a]
BC-51	72	1	3.13	0.09	27,820	240	32,540[a]
BC-55	78	1	1.09	0.11	36,290	790	41,827[a]

[a] These radiocarbon ages are beyond the INTCAL04 calibration dataset and were calibrated using the Bard polynomial (Bard, 1998).

units (Fig. 2). The basal unit occurs from the bottom of the core to almost 61 cm in depth, and consists of a homogeneous reddish-brown (5YR 3/4; 4/4) sandy clay. It underlies a well laminated second unit composed of alternating subangular quartz sand (7.5YR 6/4; 6/6) and relatively more clay-and organic-rich layers (7.5YR 3/4; 4/3) containing fragments of straws fallen from the cave roof. This second unit has its upper boundary at 48 cm, at which point a straw-rich layer is visible. $CaCO_3$ straws originated from the cave roof, occasionally falling onto the sediments [there is evidence of straw breakage on the cave's roof just above the deposit]. It should be noted that no disturbance of the sediment laminations appears to have taken place where straws have fallen. The third unit, from 47 cm to 37 cm in the core, comprises homogeneous clear quartz sand (7.5YR 6/3; 6/4). This is overlain by a distinct layer that is inferred to represent a single depositional event at the bottom of the fourth unit, which contains an unusually high concentration of straws and bones. The fourth unit is a succession of predominantly subrounded quartz sand forming a set of alternating pale (7.5YR 5/4) and more clay-rich dark layers (7.5YR 4/4; 3/4). Those layers appear to be very thin and could be considered as lenses within the larger sandier layers with the exception of a 5 cm thick layer from 27 cm to 22 cm deep. The uppermost unit consists of a 3 cm thick dark (5YR 2/2), homogeneous, clay-and organic-rich deposit.

3.2. Chronology of the deposits

3.2.1. ^{14}C chronology

A total of 25 samples were analysed, two of which were discarded because of the obvious infiltration of material down the profile despite the fact that the entire profile is clearly layered. The data are plotted in Fig. 4 (the raw data are presented in Table 1) and indicate a clear change in sedimentation rate, with relatively more rapid deposition on the top 36 cm of sediment. Sedimentation appears to have ceased at this location in the cave around the onset of the Holocene (but see Discussion below).

3.2.2. OSL chronology

The OSL age estimates and data used for age calculation are presented in Table 2. An assessment of the luminescence behaviour of the samples indicates that the Blanche Cave sediments are well suited to OSL dating using the SAR protocol. Despite the small size (<50 grains) of the aliquots, all aliquots measured yielded bright luminescence signals, with rapid decay of the signal within the first few channels indicating dominance of the fast component (Fig. 3). All aliquots yielded recycling ratios within 5% of unity and thermal transfer of <1% (Table 2). Dose distributions formed narrow populations indicating very well bleached sediment except in the cases of K2015a and K2016a. Both of these samples yielded a small proportion of older aliquots indicative of incomplete bleaching (Fig. 3; Appendix 1).

The dose rates for all samples are <1 Gy/ka (Table 2). Such low dose rates may reflect the composition of the sediment as almost pure quartz, combined with low radioactivity limestone from cave sediment inclusions. Dose rate increases down the core. This is consistent with the down-core increase in clay content. The gamma component of the dose rate was calculated using two methods for comparison; firstly using *in situ* gamma spectrometry and secondly based on ICP-MS measurements for the sedimentological units using the layer model of Aitken et al. (1985). The two sets of results proved very similar (see Section 2.3.2). This observation is significant, since it substantially improves confidence in the dose rate calculations and, therefore, age estimates overall. However, it must be considered that ICP-MS analyses were undertaken on small volumes of material, which is not ideal given the inhomogeneity of the laminated cave sediments, despite care being taken to ensure representative subsampling. Furthermore, high-resolution gamma spectrometry, which can assist with identifying disequilibrium in the radionuclide decay chains, was not undertaken on the core sediments due to the scarcity of sediment and the difficulty of subsampling laminated material, which might introduce further uncertainties.

The calculated ages for the six samples versus depth are plotted in Fig. 4. The OSL chronology, as with the radiocarbon chronology,

Table 2
Equivalent dose (Dc), dose rate data and OSL age estimates for all samples from the Blanche Cave core.

Core depth (cm)	Lab code	De (Gy)	Recycling ratio	Thermal transfer (%)	K (%)[a]	U (ppm)[b]	Th (ppm)[b]	Water content (%)	Gamma dose rate (Gy/ka)[c]	Total dose rate (Gy/ka)[c]	Age (ka) ± 1σ error
10–12	K2014a	7.6 ± 0.1	1.04 ± 0.02	0.8 ± 0.0	0.10 ± 0.01	0.25 ± 0.01	1.27 ± 0.06	3 ± 2	0.063 ± 0.006	0.30 ± 0.01	25.7 ± 1.4
22–25	K2015a	9.6 ± 0.1	1.04 ± 0.01	0.5 ± 0.0	0.11 ± 0.01	0.29 ± 0.01	1.66 ± 0.08	3 ± 2	0.095 ± 0.005	0.35 ± 0.01	27.6 ± 1.3
39–44	K2016a	11.6 ± 0.1	1.03 ± 0.02	0.4 ± 0.0	0.77 ± 0.04	0.19 ± 0.01	0.92 ± 0.05	3 ± 2	0.125 ± 0.006	0.82 ± 0.05	14.2 ± 0.9
47–51	K2017a	17.7 ± 0.2	1.01 ± 0.02	0.5 ± 0.0	0.22 ± 0.01	0.67 ± 0.03	4.61 ± 0.23	3 ± 2	0.098 ± 0.005	0.54 ± 0.02	33.0 ± 1.5
62–66	K2018a	29.9 ± 0.4	0.99 ± 0.03	0.4 ± 0.0	0.28 ± 0.01	0.72 ± 0.04	6.37 ± 0.32	15 ± 5	0.181 ± 0.009	0.64 ± 0.03	46.6 ± 2.5
75–79	K2019a	41.1 ± 0.5	1.00 ± 0.02	0.5 ± 0.0	0.29 ± 0.02	0.66 ± 0.03	6.31 ± 0.32	15 ± 5	0.214 ± 0.009	0.67 ± 0.03	61.1 ± 3.2

[a] Measured by XRF, Research School of Earth School of Sciences, Australian National University.
[b] Measured by LA-ICPMS, Research School of Earth Sciences, Australian National University.
[c] The cosmic ray component of the total dose rate is 0.10 ± 0.01 Gy/ka for all samples. Cosmic dose rates took into account the thickness of the cave roof (5.6 m), depth of samples within the core, sediment density, altitude, latitude and longitude.

reveals a trend of increasing rates of sedimentation in the upper portion of the core, and also lacks Holocene sediments. However, as illustrated by Fig. 4, the OSL age estimates consistently overestimate the radiocarbon dates. Possible reasons for this chronological discrepancy are discussed in Section 4.1.

3.3. Grain size

Mean grain size analyses for the different units are plotted in Fig. 2.

Unit 1 is typically equally bimodal with a mean at ~25 μm and another ~200 μm, both at ~4–5%. Unit 2 is also bimodal around the same grain sizes but the 200 μm is a bit above 9% and the ~25 μm at ~2%. Unit 3 is almost unimodal with a 200 μm peak of 11.5% and a 25 μm of <1%. The particular layer at the top of the latter unit returns to the pattern found in unit 1 with the ~25 μm peak reaching a bit more than 4% and the ~200 μm a bit less than 4%. Unit 4 resembles unit 2 with a strong peak at about 300 μm (~10%) and a much smaller one around 25 μm (~1%). Unit 5 is completely different from the other units; it shows a broad, unimodal peak around 20 μm (close to 6%) and a smaller one (~1%) around 200 μm. The broad peak is asymmetrical and displays values above 2% within the 3–10 μm range.

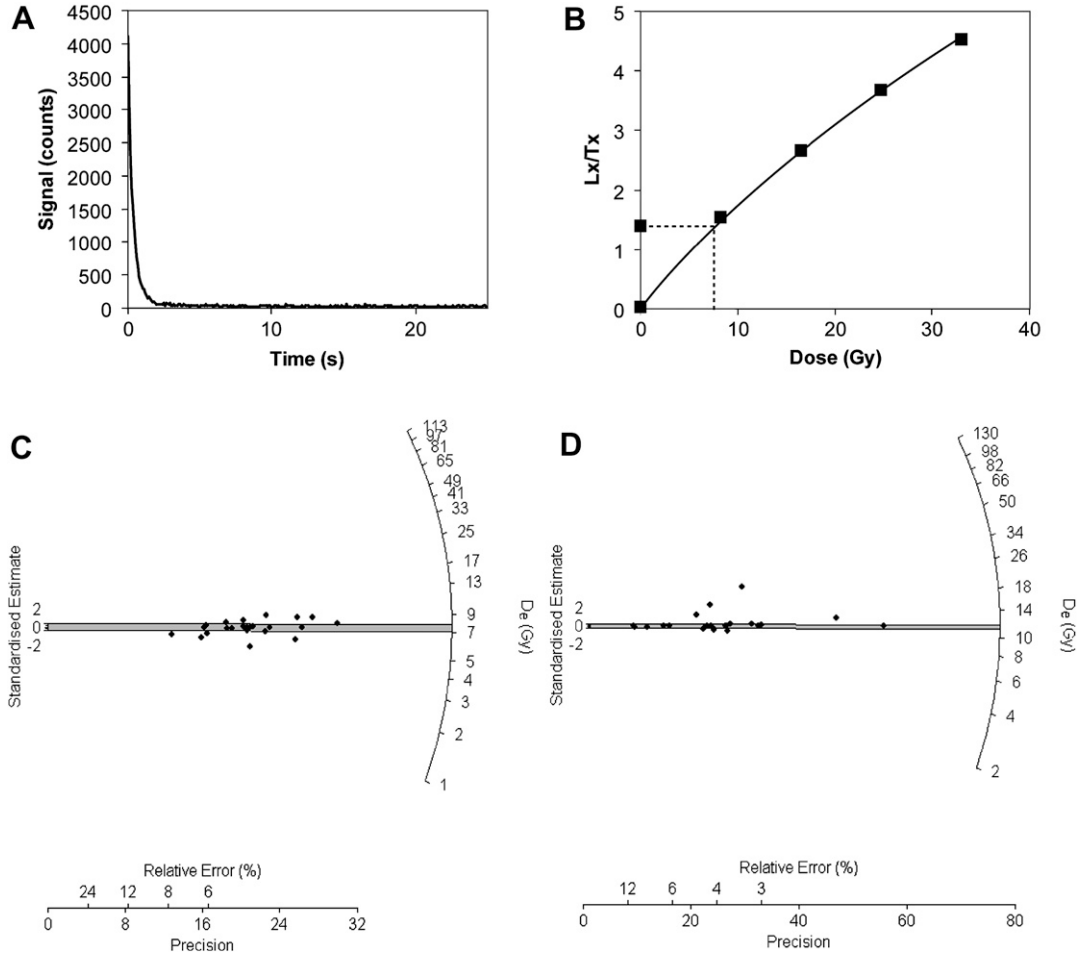

Fig. 3. Examples of luminescence characteristics for Blanche Cave aeolian quartz: A. Luminescence signal arising from one aliquot of sample K2014a, showing bright signal, rapid decay and dominance of fast component; B. Dose-response curve for one aliquot of sample K2014a, illustrating simple exponential growth of sensitivity-corrected signal with regenerative dose; Radial plots for sample K2014a (C) and K2016a (D), showing narrow dose distributions indicating generally well bleached sediments.

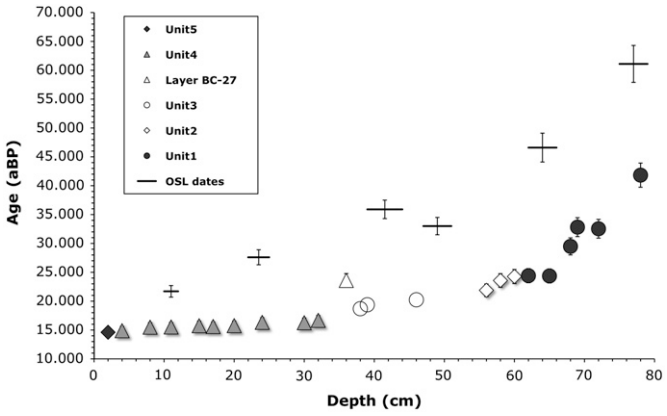

Fig. 4. Plot of the calibrated radiocarbon ages superimposed on the OSL ages versus depth for the core from Blanche Cave.

3.4. Grain morphology

Four main morphologies were identified under scanning electron microscopy (Fig. 5). These are specific to particular units recognized in the core.

The broad unit 1 contains grains that characteristically show obvious signs of etching and are also subangular (see Fig. 5, 21–28). Unit 2 consist of grains that are rounded to subrounded compared to the basal unit. Unit 3 is unique for the core in that the grains are rounded (Fig. 5, 14–20) and display a very smooth pattern with occasional pits (Plate I, 16–19). The layer BC-27, at the bottom of unit 3 consists of grains that are subangular to subrounded (Fig. 5, 11–13), with some that display obvious etchings marks, as seen in unit 1 (Fig. 5, 11). Unit 4 is composed of grains that are subangular to angular (Fig. 5, 5–10) but are less smooth than grains in unit 3. Unit 5 yields many subrounded grains that are much smaller and with multiple coatings. There is no sign of smoothing (Fig. 5, 1–4).

3.5. Geochemical analysis

Various elemental ratios are plotted in several diagrams for the 5 different units recognized in the core. A distinct but narrow layer below 35 cm in the core (labeled BC-27) was also geochemically analysed. Plots of selected ratios are presented in Fig. 6.

The major element data show that many elements are strongly anti-correlated with Si (Fig. 6). In contrast, Ca, P, and S are positively correlated, as are Mg and Al, except that in the basal unit (1) two values are out of trend (Fig. 6k and l). When these two anomalous values are excluded, the correlations follow the trend for the entire core. The basal unit 1 is particularly rich in Ca and P. Some of the highest SO_3 measurements were also obtained from that unit, and two levels enriched in straws (BC-27 and 34). Several trace elements such as La and Y also show good correlations with Si, always with elemental values decreasing when Si values increase (see Fig. 6b–e).

However, the plots of Zr/Ti versus Si indicate a poor correlation (Fig. 6f) despite Zr/Ti seeming to increase proportionally with an increase in percentage of Si. The same applies for the Sr/Ca versus Si (Fig. 6g).

With respect to major elements, there are good correlations between Al and Mg (Fig. 6h), Ca and P and S and Ca (Fig. 6i and j) except that in the basal unit (1) two values are out of trend, but when eliminated (Fig. 6k and l) the correlations follow the trend for the entire core.

Rare Earth Elements display good to extremely good correlations: Sr versus Nd (0.7005), Gd versus Pr (0.9976), Dy versus Pr (0.997), Sm versus Gd (0.9985), La versus Rb (0.9557) and Cs versus Y (0.95), with the clay-rich units always showing the highest concentrations (see Fig. 7a–f). These correlations apply for other REEs as well.

The binary plot presented in Fig. 7 illustrates the distinct concentrations in REEs between the two different main types lithologies recognized in the core: the clayey layers and the sandy layers. All the REEs concentrations have been normalized versus concentration values obtained for PAAS (Post-Archean average Australian Sedimentary rock; McLennan, 1989) in order to compare each sample on the same basis. Even if all the units show a similar pattern, the clayey layers display much higher concentrations in RREs and the sandy layers are less concentrated as they show values ranging from 5 to 20 ppm/ppm PAAS.

Nd isotopic compositions display a narrow range of values with εNd spread between −9.91 and −12.80 (see Table 3 and Fig. 8). The more sandy horizons generally display more negative values, indicating that those layers contain an isotopically distinct component compared to the clayey units, which principally occur at the base of the section as well near the top.

3.6. Pollen evidence

A total of 20 samples was analysed for their pollen and charcoal contents. Twenty-nine distinct pollen groups were recognized, in addition to both monolete and trilete spores. Of note is the presence of the exotic [to Australia] *Pinus* pollen in the top 2 samples in the sequence which are found in the dark brown unit 5. Charcoal particles were also found in all samples. Five samples were devoid of pollen and come mainly from the reworked layer [BC-27] as well as unit 3 and one additional sample at the units 2–3 boundary. The full palynological presentation and interpretation of the record from Blanche Cave will be presented elsewhere (Reed and van der Kaars, pers. comm.). Here, we present the broad trends (Fig. 9) of importance to the environmental interpretation associated with the geochemical data and the nature of the vegetation during phases of sediment mobility outside the cave. Accordingly, we are presenting a summary diagram of the palynoflora by grouping all the taxa into 3 main groups: (1) Woody taxa; (2) Woody–herbaceous taxa, and (3) Herbaceous taxa. Aquatic taxa and ferns are plotted and tabulated separately. The basal portion of unit 1 shows some woody taxa that are being replaced by herbaceous taxa at 29 ka. Unit 4 sees a progressive drop in herbaceous taxa to the benefit of woody taxa. This is accompanied by the appearance of aquatic taxa, although numbers are low.

4. Discussion

4.1. Chronology

A recent publication by St Pierre et al. (2009) which discusses Uranium-series dating of straws from the same deposits and which also uses our ^{14}C dates, shows a fairly good correlation between U-series ages and ^{14}C analysis on charcoal particles. In the upper part of the profile, however, the straws yield Holocene ages (3.0 ± 0.14; 4.8 ± 0.86 and 4.6 ± 0.35 ka BP). These samples are substantially younger than ^{14}C dates from the same part of the core. At the same depth (at 5 cm), where the first date was obtained, three additional dates yield much older U-series ages (236 ± 15; 264 ± 8.0; 56.1 ± 5.1 ka BP). This mixed assemblage of dates indicates that anthropogenic disturbance could have caused some straws to fall from the roof of the cave and become mixed in the upper part of the profile. No other straws older than the Holocene were found lower

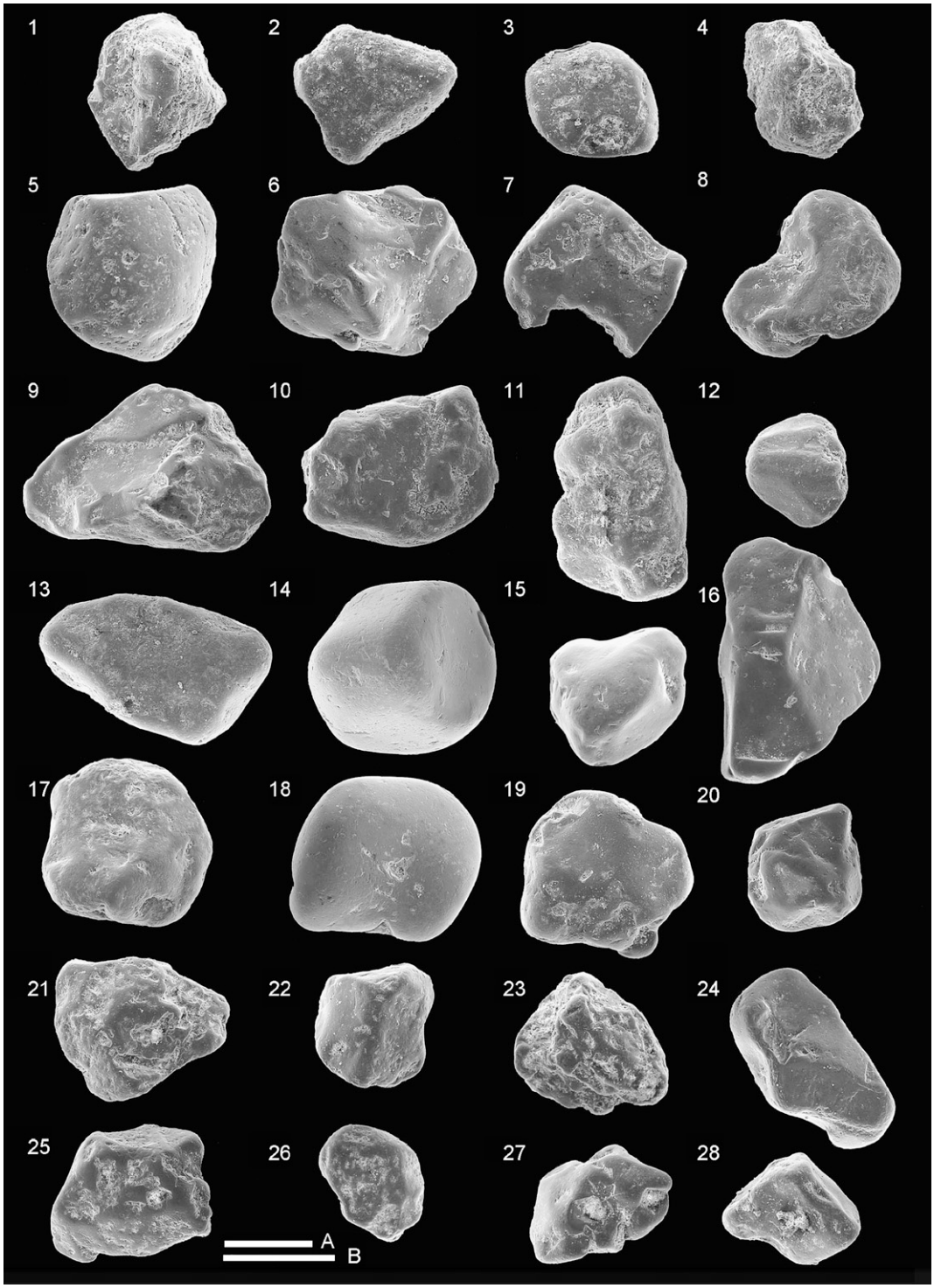

Fig. 5. Scanning electron microphotographs of individual quartz grains recovered from the Blanche Cave core. Scales A and B: 400 μm. Scale B is assigned to grains 1–21, 23, 25 and scale A to grains 22, 24, 26–28. Unit 5 is from grain 1 to 4, Unit 4 from 5 to 10, Layer BC-27: 11–13, Unit 3: 14–20 and Unit 1: 21–28. Unit 2 is not represented.

down the profile. Neither the charcoal ^{14}C nor the OSL chronologies from this study indicate Holocene deposition, and for this reason, we disregard the Holocene U-series ages for the upper part of the profile.

There is no clear explanation for the absence of Holocene sediments at the core site except for a possible change in drainage direction, or cave floor slope, which would have resulted in sediments being transported to other parts of the cave during the Holocene. The more plausible explanation is that human excavation of guano, which would have removed the upper (Holocene) surface of the cave floor, took place in this region. Indeed, bat guano was mined from several Naracoorte caves for agricultural purposes between 1871 and 1897 (Hamilton-Smith, 1998). At the rear of the third chamber of Blanche Cave is a large pit that was associated with mining activity (Hamilton-Smith pers. comm. 2005). Several other locations within the cave show evidence of guano extraction. As the bats currently use the area adjacent to the dig site for winter roosting

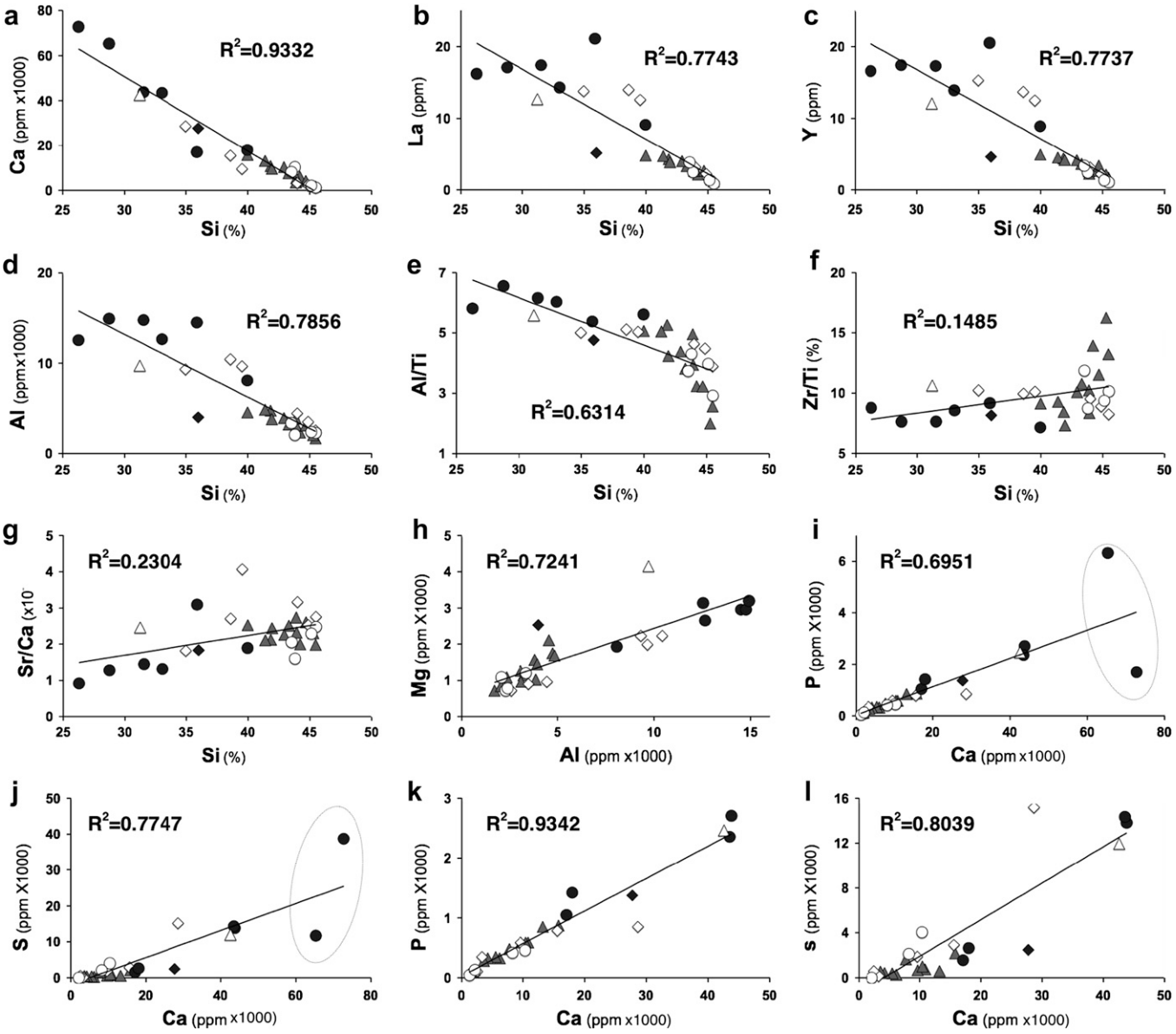

Fig. 6. Binary plots to show the differences in elemental composition for the different units from the Blanche Cave core. For symbols, refer to Fig. 11. Different ratio plots are provided in a to l but, in plots i and j, 2 extraneous values for unit 1 are highlighted in an ellipse and those points have been eliminated in the corresponding plots k and l that then show better correlations for P/Ca and S/Ca.

and caves sediments at Naracoorte are known to be guano rich (Forbes and Bestland, 2006), it is reasonable to suggest that the uppermost units at the excavation site may have been removed during mining. Furthermore, contamination due to anthropogenic activity in the upper part of the core is supported by the presence of *Pinus* pollen in the topmost unit 5 (Fig. 9), which is also richest in dark brown humic material. There is a marked discrepancy between the ages obtained from the two dating techniques. The OSL age estimates are consistently older than the corresponding radiocarbon dates from corresponding depths down the core. In the upper part of the profile, there is approximately 10 ka difference between ^{14}C and OSL (Fig. 4). This difference increases to approximately 25 ka lower down the profile. However, both suites of ages show the same broad trend of deposition, with slow deposition for the lower ~40 cm, and an increase in sedimentation in the upper ~40 cm of the core.

To examine the potential sources of discrepancy, it is necessary to examine the veracity of both dating techniques at this site. The radiocarbon results suggest no contamination of the samples. There is no indication from the measurements that material has been incorporated from above or below the sampling points, nor from the laminations within the sediment. However, it may nevertheless have been possible for water containing humic acids to have infiltrated sediments deposited much earlier, which would result in apparently younger dates than the deposition of the sediment itself. We do not think this to be a possibility since the radiocarbon ages clearly conform with the U-series ages obtained from the straws [see Fig. 7 in St Pierre et al. (2009)]. With respect to the OSL samples, the quartz luminescence behaviour indicated suitability for OSL dating using the SAR protocol (see Section 3.2.2). The two methods used to calculate the gamma component of the dose rate yielded comparable results. Despite this, the OSL ages consistently over-estimate the radiocarbon dates. This observation raises some concern about the accuracy of the dose rate calculations, and therefore of the OSL age estimates, particularly since age

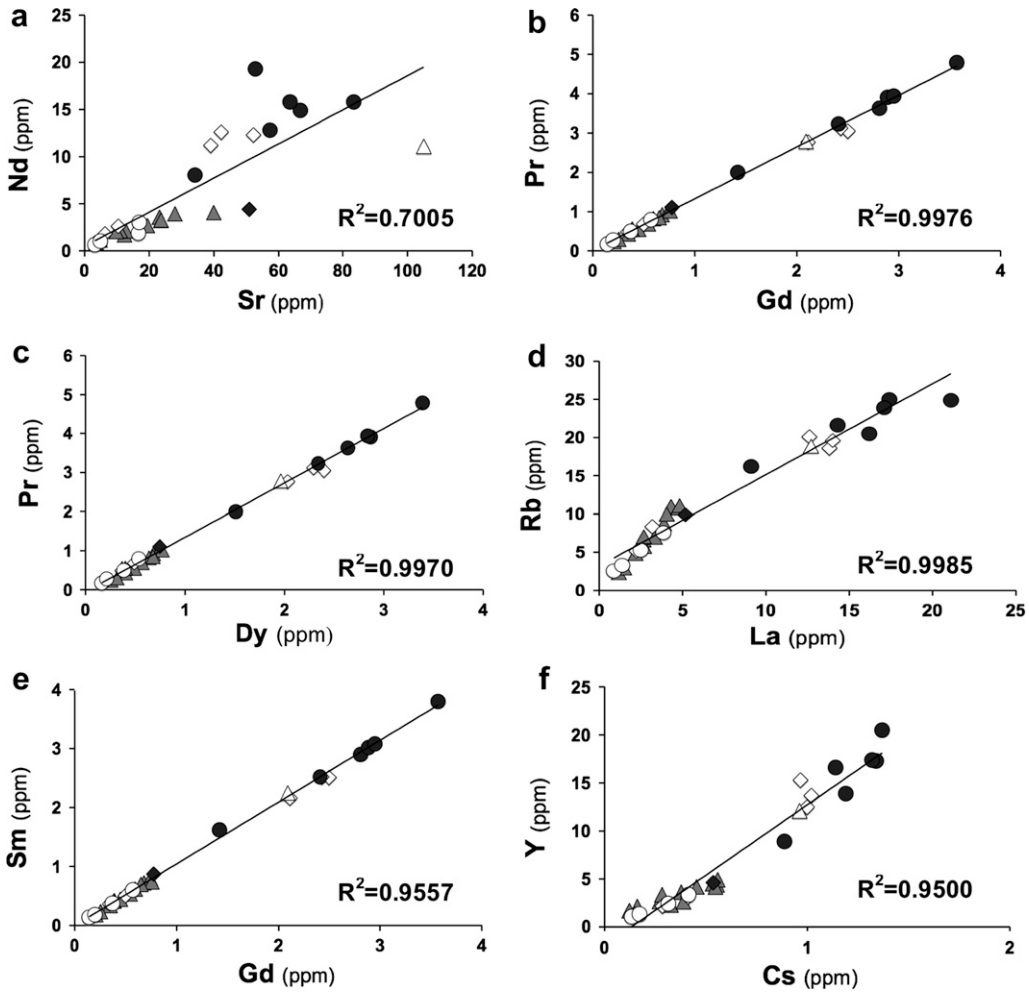

Fig. 7. Binary plots to show the differences in REE composition for the different units from the Blanche Cave core. For symbols, refer to Fig. 11. Note that many plots return extremely high correlation coefficients. For more details, see text.

calculation for OSL is complex. For example, it is possible that dose rate disequilibrium took place through time, resulting in inaccurate dose rate estimates and associated apparently older ages. However, since the dose rates are comparable with one another irrespective of different methods of calculation involving independent analytical techniques, it is difficult to explain the consistent and systematic over-estimation. It is possible that the discrepancy between the two chronologies is not solely due to problems calculating the OSL dose rates; a process-based explanation for the disparate chronologies must also be considered. The chronologies are assumed to explain the timing of sedimentation at the core site, which is located 50 m from the site of roof collapse. It has also been assumed the OSL signal was reset as the sediment blew in from the cave opening, but this assumption may be incorrect. The OSL signal may have been reset as the sediment was deposited onto a dune on the surface, rather than when it was blown into the cave. However, this model is unlikely, given that there is no evidence to suggest incomplete bleaching in the sediments (Fig. 3; Appendix 1), and the consistency of OSL age over-estimation relative to radiocarbon dates would require this to have taken place for every sample,

Table 3
Nd isotope analysis of several samples from the Blanche Cave core.

Sample number in core	Depth (cm)	143Nd/144Nd	2SE	EpsNd	Cal. age aBP (inferred in italics)
BC-2	2	0.512098	0.000016	−10,534	14,608
BC-4	4	0.512102	0.000018	−10,456	14,887
BC-9	11	0.512021	0.000009	−12,036	15,529
BC-13	17	0.511982	0.000007	−12,797	15,614
BC-18	24	0.512050	0.000016	−11,470	16,326
BC-21	28	0.512049	0.000010	−11,490	*17.020*
BC-26	34	0.512018	0.000007	−12,094	*18,061*
BC-31	43	0.511993	0.000018	−12,582	*18,581*
BC-33	46	0.512027	0.000012	−11,919	18,929
BC-39	56	0.512030	0.000013	−11,860	21,880
BC-42	60	0.512022	0.000013	−12,016	24,271
BC-48	68	0.120900	0.000008	−10,690	29,489

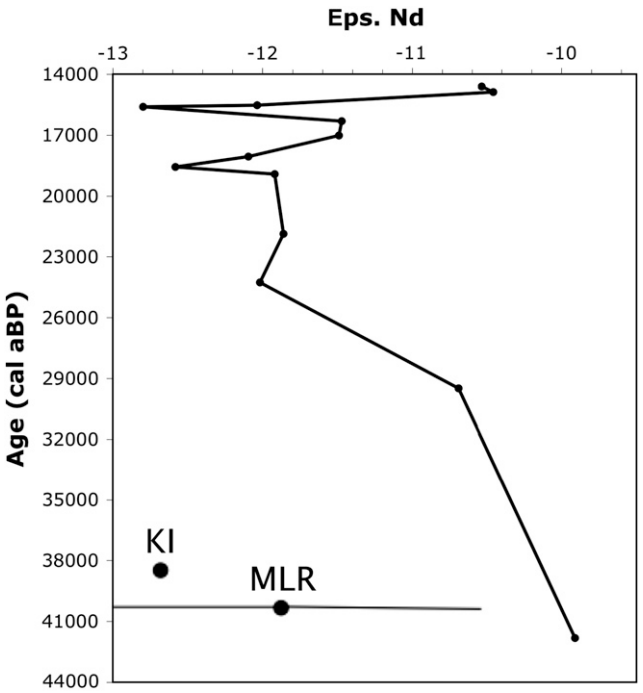

Fig. 8. Plot of the Nd isotopic composition [as εNd] versus depth in the Blanche Cave core. There is also indicated the εNd values obtained by Turner et al. (1993) for the Mount Lofty Ranges (MLR) and Kangaroo Island (KI).

which is unlikely. Alternatively, the OSL signal may have been reset as material was blown into the cave opening, but that sediment may subsequently have taken a long time to be transported down the gentle slope of the cave floor to the core site, during which time the signal was not reset, resulting in comparatively older OSL ages than for radiocarbon. However, this model is also unlikely considering the conditions in the cave and laminated nature of the sediments. It is therefore necessary to consider the fact that U/Th dating of straws, derived from the roof of the cave and which fell onto the cave floor and were subsequently incorporated into the sediments, indicate similar ages to those obtained from radiocarbon analysis of charcoal (St Pierre et al., 2009). This, combined with the systematic (albeit as yet unexplained) over-estimation of the OSL ages relative to ^{14}C, leads us to consider the ^{14}C ages to be the most plausible for the dating of the core. We assume this to be the correct one until a better explanation is obtained for the age discrepancy.

4.2. Grain morphology and size

It is clear that the 5 units including the layer BC-27 that were distinguished at first on colour and lithology were further confirmed on many aspects of grain sizes, morphologies and geochemistry. Based on grain size and morphology, unit 1 (41.8 ± 0.8–24.4 ± 0.1 ka cal BP) yields the lowest quantity of quartz to the detriment of phosphatic and sulphate minerals. The phosphatic component consists of two end members: bones of microvertebrates and bat guano, as already recognized by Forbes and Bestland (2006) in Blanche Cave and other Naracoorte caves. The etched nature of the quartz grains in this unit is puzzling as we are not sure if the etching is post sedimentary. However, etched quartz is present in the acidic podsol above the cave. That could plausibly be the source for the etched grains we found. Wetter conditions during or postdating the deposition of this unit would surely explain the presence of gypsum in this unit. Pollen recovered from the same unit indicates wetter conditions compared to

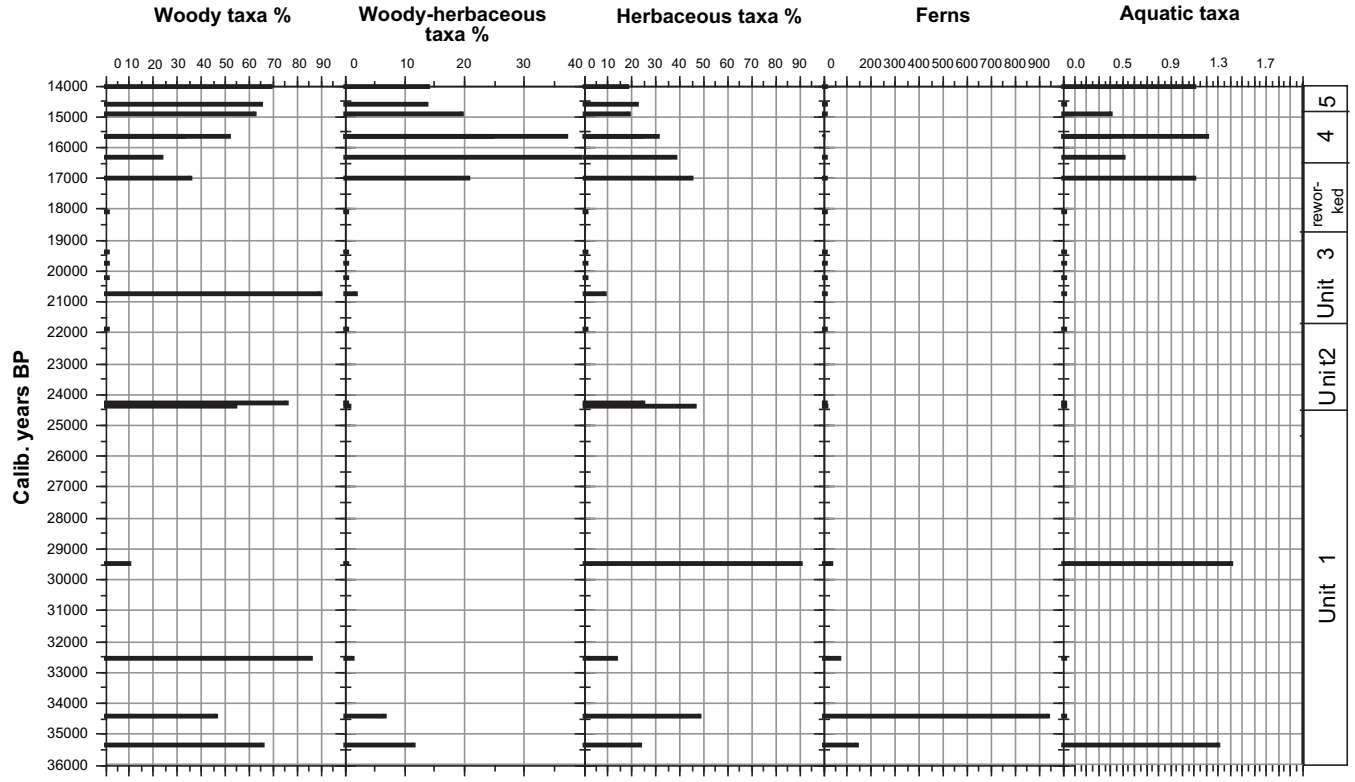

Fig. 9. Abridged pollen and spore diagram for the Blanche Cave core. Woody taxa, woody–herbaceous taxa and herbaceous taxa are plotted as percentages of the total pollen counts. Plots of *Pinus*, ferns spores [combining monolete and trilete spores] as well as the presence of aquatic taxa are represented for absolute counts. The chronology used here relies on radiocarbon dates from charcoal particles. On the right hand side, the extent of the different lithological units is defined.

today and the rest of the core (see Fig. 9). Unit 2 (24.3 ± 0.1–21.8 ± 0.1 ka cal BP) is transitional between the basal unit and unit 3 (21.8 ± 0.1–18.7 ± 0.1 ka cal BP) which was deposited during the Last Glacial Maximum (LGM) and consists of much larger grains and very well rounded ones. This implies stronger wind conditions and that the grains have been transported over longer distances. Unit 2 displays alternating conditions identified by the alternation of layers of different nature. The layer BC-27 very likely represents a single phase of deposition that consists of reworked material from unit 1 as shown by similar grain morphologies (e.g. etched grains and grain size spectrum, as evidenced by the radiocarbon age (non calibrated) of $20{,}010 \pm 110$ aBP). The event at the origin of the rework of some material from unit 1 must have occurred between 18.7 ± 0.1 and 16.7 ± 0.1 ka cal BP. It is likely that it results from an erosive process that occurred elsewhere in the cave and that was redeposited at the studied site. Unit 4 (16.7 ± 0.1–14.9 ± 0.1 ka cal BP) points to a return of conditions similar to those of units 2 and 3. Unit 5 is considered to result from anthropogenic changes in the landscape caused by agricultural practices. This horizon relates to different aeolian conditions and a change of sedimentation rate. The organic nature of the sediment obviously relates to soil erosion in the catchment of the cave at least and *Pinus* pollen clearly points to the European phase. We ought to consider that the top 5 cm of the core [representing the upper layer of the cave floor] must have been disturbed by people walking in the cave since its discovery.

With respect to grain size, the different units can equally be differentiated. Unit 1 displays a bimodal distribution that is not recognized elsewhere in the profile, except for the reworked layer BC-27. This further confirms that the latter layer originates from unit 1. The two peaks centred around 200 and 20 μm are of almost equal amplitude. Unit 2 can divided into 2 separate sub-units which alternate: the clayey layers (see Fig. 2) show a similar pattern to unit 1 but with a smaller amount of material peaking around 20 μm, but contains a certain amount of fines. The sandy sub-units consist almost entirely of grains peaking around 200 μm. Unit 3 is equally abundant in grains peaking around 300 μm with very few fine particles. Unit 4 returns to conditions similar to those of the sandy layers seen in unit 2 with an obvious peak >200 μm and a sub-peak around 25 μm. Unit 5, on the other hand, is very different from the other units by being almost unimodal with a large amount of particles centred around 20 μm. It is noteworthy that all the units that have a strong peak around 200 μm (sandy layers in unit 2, unit 3 and unit 4) yield values for quartz above 92.5%. This implies close proximity of quartz sand dunes to the cave. Units 1 and 5 imply a certain amount of aqueous transportation. Quartz grains from units 4, 3 and 2 clearly display a high level of roundness (see Fig. 5) as anticipated from dune fields that have undergone a high level of transport and reworking.

4.3. Geochemistry

The 5 units and the reworked layer BC-27 are clearly fingerprinted by a series of major and trace element characteristics. In addition, the quartz-rich layers are easily separated from those that contain finer (clayey) fractions as shown by the PAAS-normalized REE diagram (Fig. 10) as well as the Nd isotopes. Those geochemical fingerprints further confirm our separation of the core into the different units.

The spider plot shows that, for unit 2, three sandy layers are easily distinguishable from the 3 clayey ones. The concentration of the REEs in the less sandy units is higher than in the sandy units/layers and points out to a different provenance.

Overall, there are two groupings with respect to trace elements for the entire core. These are clearly displayed in Figs. 6, 7 and 10 and will be further discussed below, when identifying the origin of the material from the 5 different units.

Many of the elemental ratio plots presented in Figs. 6 and 7 clearly indicate that the five different units can be distinguished from one another on geochemical grounds. Unit 5 is clearly different from the others and points to a different origin. Layer BC-27 is frequently associated geochemically with unit 5, further confirming the reworked nature of this particular layer and its origin from unit 5.

The P/Ca and S/Ca ratios again indicate the presence of high amounts of guano and gypsum in unit 5 (see Fig. 6i–l).

The variation in major and trace elements primarily reflect mixing of quartz and clay. However, variations in key trace element ratios such as Al/Ti, REE patterns, and Nd isotopic composition show that the range of element concentrations cannot simply reflect mixing of quartz with clay having a single composition. The clay component, which controls most of the element abundances, must also be changing in composition between the quartz-rich and clay-rich layers. This suggests that distinct source terranes must be contributing to the clay layers, and that these variations in clay provenance vary in synchrony with the abundance of quartz.

The REE composition of the different units clearly differentiates Unit 4 (and 5) from the rest of the profile as evidenced in Fig. 10. However, as we postulate that there is a likely possibility that the bottom portion of the profile at Blanche Cave may have been inundated [see discussion below] during a period of higher water table during a much wetter climate, it is possible that local 'contamination' from the local lithologies may have affected sediments and its composition in the bottom unit.

Based on the results of our geochemical analyses, in combination with the Nd isotope ratios, we propose a likely origin for the sediments in Blanche Cave which is in contradiction with the one put forward by Forbes and Bestland (2007).

Indeed, our data suggest that the major part of the deposit in the Blanche Cave core came from the north western region of South-East South Australia. More precisely, the Kanmantoo Trough, which forms the eastern part of the Mount Lofty Ranges gives Nd isotopic ratios encompassing the most part of the core ($\varepsilon Nd = -11.87 \pm 1.27$ – Turner et al., 1993). In addition, the εNd for Kangaroo Island determined by Turner et al. (1993) points out the same range of values ($\varepsilon Nd = -12.7$) thus indicating that, especially during drier phases (in the core, $\varepsilon Nd = -12.8$ at 15.6 ka and $\varepsilon Nd = -12.6$ at 19.9 ka), the sediment deposited in the core came from this region, further afield North West of Naracoorte.

These results are further confirmed by the comparison of the geochemical composition of the core to the surrounding soils (see Fig. 11) as determined by Mee et al. (2004). Those authors identified

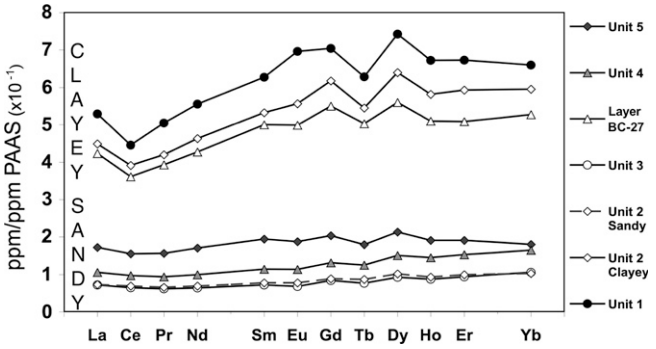

Fig. 10. Spider plots for mean values for REEs for the different units as well as the reworked layer BC-27 analysed for the core taken in Blanche Cave. The data are normalized against the PAAS. The contrast between the two main compositions of the layers of the core (sandy and clayey) is clearly distinguishable.

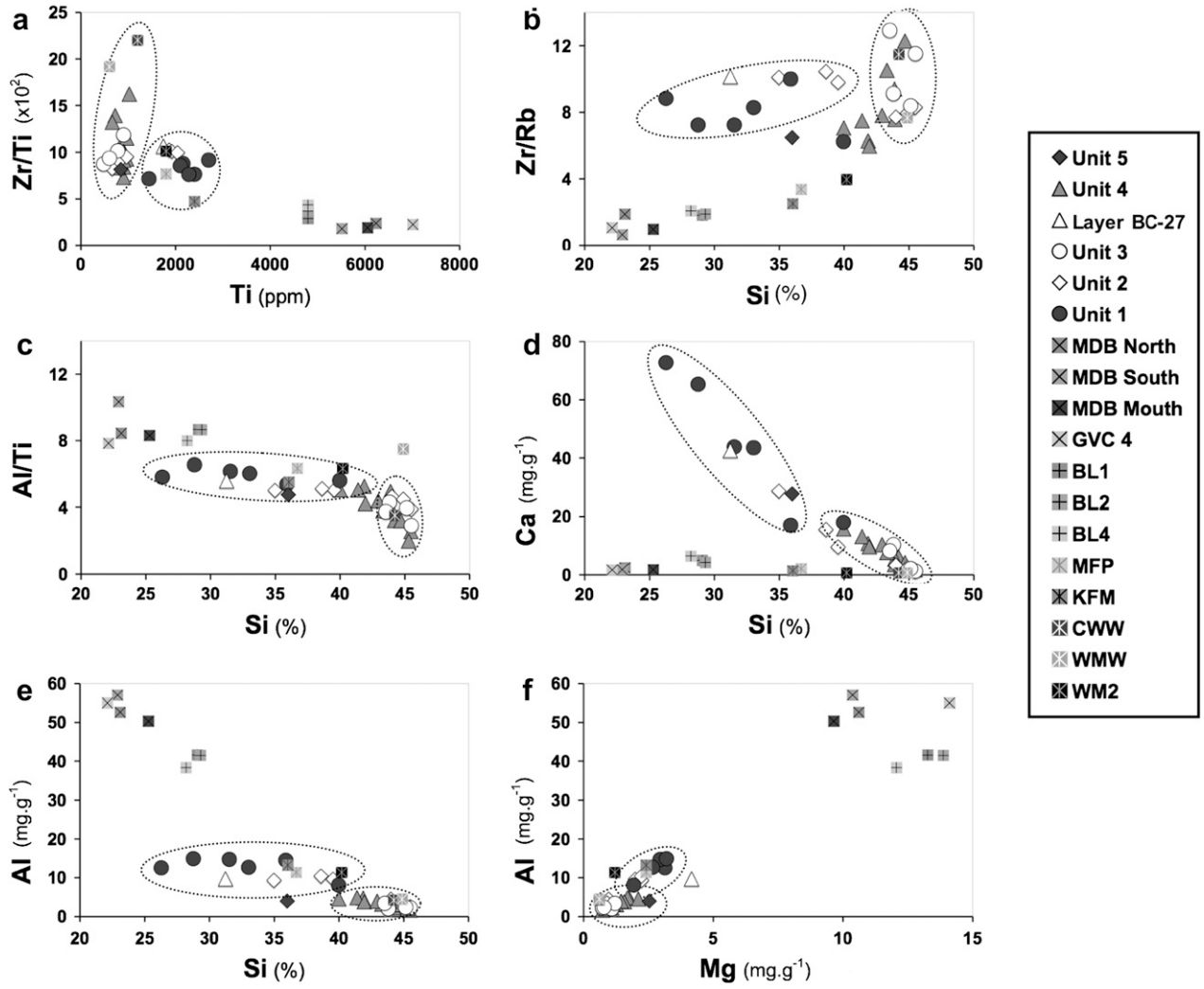

Fig. 11. Binary plots for selected elements representative for the 5 units recovered in the Blanche Cave core for comparison with other surficial deposits in South Australia in an attempt to determine the origin of the aeolian material. MDB: Murray-Darling Basin; GVC 4: from the Onkaparinga River, south of Adelaide (see data in Gingele and De Deckker, 2005); BL1-4: Bool Lagoon lunettes; MFP: Meningie floodplain Coorong; KFM: Kingston floodplain; CWW: Wood Wells Coorong; WMW: Wellington silty sand (west); WM2: Wellington silty sand (east) (see data in Forbes and Bestland, 2007).

that the origin of the Terra Rossa soils in the vicinity of Naracoorte is from the Kanmantoo Shales on Kangaroo Island and the Fleurieu Peninsula. Here, we show a good correlation between the sediments from the core and the deposits from Wellington silty sand, the Meningie floodplain as well as the Wood Wells that are areas situated around the Mount Lofty Ranges, the Coorong and the Padthaway Ridge.

These results are consistent with the presumed winds coming from the NNW in this part of Australia for the glacial period as identified by Sprigg (1979; Fig. 17).

In contrast, our data show no correlation with any site located along the Murray and Darling rivers sampled by Gingele and De Deckker (2004), as well as any other immediate Naracoorte surrounding soil (e.g. Bool Lagoon Lunettes as described by Forbes and Bestland, 2007). Our findings for the origin of Blanche Cave sediments which contrast with these of Forbes and Bestland (2007) could be explained by the fact that their conclusions are primarily based on Sr isotope analysis which could be influenced also by the local signal from the limestone which makes the caves. This is the reason why we did not perform Sr isotope analysis on the Blanche Cave sediments.

5. Conclusion

The lower part of the profile at Blanche Cave was formed during the period which preceded the Last Glacial Maximum [=LGM], namely Marine Isotopic Stage 3, a time when SE Australia was very wet and lakes were exceptionally high as best exemplified with the full lake levels in the Willandra lakes area in western New South Wales (Bowler et al., 2007). Near Blanche Cave, woody taxa ranged in abundance between 67 and 85%. Ferns were present in the cave, but this is explainable due to the sheltered nature of this setting. [Note that ferns are common in the cave today and that bracken ferns are a very common part of the under storey in native bushland near the cave]. During that time, sediment accumulation at Blanche Cave was very high. Afterwards, with climate gearing to the LGM, sedimentation rate decreased somewhat with herbaceous taxa increasing in percentages, except for one level at ~20.8 ka when woody taxa reached 90%. Following the LGM, woody–herbaceous taxa increased in abundance and this is concordant with data available elsewhere that the deglaciation coincide with wetter conditions that favoured a vegetation cover over the landscape (see Harle, 1997 for discussion).

Mean grain size analysis profiles (Fig. 2) show a nice two-component system with the smaller component having a modal size of about 23 μm, and the larger one varying between 100 and 220 μm. It could indeed be argued that one of those is aeolian and the other was generated under aqueous conditions; this is not surprising as water would have entered in the cave at times, and also because conditions in caves in general are quite humid in any case. In addition, as the silica content of the samples with the coarser mode is highest, it would seem reasonable to assume that this is quartz-rich airborne material. Another support for this interpretation comes from the microscopic observations that show particles in these size ranges to be nicely rounded with also some pitted surfaces.

Grain size morphologies and textures indicate that the lower unit in the cave shows some partial dissolution that must have affected the quartz grains. The presence of sulphate in unit 1 implies the presence of gypsum paralleled with high phosphate levels, likely to have been brought in by the large amount of guano. It is possible that the water table in the cave was significantly higher than today and that the deposit was immersed in water. In contrast, unit 3 which almost completely coincides with the LGM, displays quartz grains that are well polished and very well rounded. This implies a very different wind regime, likely to have been more substantial to transport these quartz grains from a further distance, implying a drier climate with little vegetation cover.

Many of the elemental ratio plots presented in Figs. 6 and 7 clearly indicate that the 5 different units can be distinguished from one another on geochemical grounds, although Nd isotopic ratios clearly indicate that the origin of the cave sediment is the Kanmantoo Group from the NW and NNW, principally from the Mount Lofty Ranges and the Padthaway Ridge. It is likely that this origin applies for the line-grained sediment.

In addition, ellipses in Fig. 11 group those samples from the Blanche Cave profile which share some geochemical affinity with others from other regions, on the basis of particular elemental ratios. These plots reaffirm the distinct nature of individual Blanche Cave units.

For example, the clayey layers of units 1 and 2 have a chemical composition resembling those from the Kingston Floodplain, the Meningie Floodplain near the northern end of the Coorong and to a lesser extent the Wellington silty sand (east) (see data from Forbes and Bestland, 2007). These are principally based on Al/Si, Mg/Al and Zr/Ti versus Ti.

In contrast, for the sandy layers in units 2, 3 and 4, the geochemical similarity with Woods Well region adjacent to the Coorong, Wellington silty sand (west) (see data from Forbes and Bestland, 2007) is very clear as shown in all the plots in Fig. 11 (e.g. (a) Zr/Ti versus Ti; (b) Zr/Rb versus Si; (c) Al/Ti versus Si; (d) Ca versus Si; (e) Al versus Si, and (f) Al versus Mg).

Based on elemental ratios, unit 5 is distinguishable from the other units of the profile and from the regional regolith. No clear origin for this unit has been found thus far, but we must acknowledge that it has undergone some anthropogenic alteration. Nd isotopic ratios further confirm the unique nature of unit 1 from the rest of the cave profile.

It is also noteworthy that none of the geochemical fingerprinting of the clay fraction determined by Gingele and De Deckker (2005) from the River Murray link with the Blanche Cave profile (Fig. 11). Overall, the likely source of the aeolian material deposited in Blanche Cave comes from NW of Naracoorte, spanning from Meningie to Kingston for the entire deposition of the profile.

During wet phases (units 1, 2-clay layers), the postulated origin is from the Wellington silty sand east, and even more so from the Kingston Plains. During drier phases (units 2–sand, 3 and 4) that encompass the LGM, the aeolian material originates from the Wellington area and Meningie Floodplain. This indicates a slight change of predominant wind direction through time spanning the period of ~41,000 to 16,000 years. The geochemical nature of the lunettes associated with Bool Lagoon, SW of Naracoorte clearly eliminates this area as a supplier of material to Blanche Cave. This is in contrast with what was postulated for the origin of the sediment found in Robertson Cave and Wet Cave by Forbes and Bestland (2007).

If we were to use the OSL chronology instead of the radiocarbon chronology based on charcoal currently accepted in this paper, the interpretation of the origin of the aeolian material would not change, but simply the timing of events, with a postulated age at the bottom of the core extending to ~61 ka. However, a recent study using U-series to date speleothems from Blanche Cave (St Pierre et al., 2009) is highly coherent with the ^{14}C dates presented here and seems to support the radiocarbon rather than the OSL chronology.

Acknowledgements

LR acknowledges funding for the pollen analysis, OSL dates and radiocarbon dating and palaeontological research provided by the Australian Government through the NHT World Heritage funding program. PDD acknowledges financial support from ARC Discovery grant DP0772180. We are also grateful to Dr J.-B. Stuut for discussion on the significance of the grain size analysis profiles.

ND is grateful to M. Cremer for access to the grain size analyser at the University of Bordeaux I and for his advice. KEF acknowledges the assistance of T.T. Barrows with the collection of gamma spectrometry in the field, and would like to thank H.M. Roberts, F. Davids and R. Grün for valuable discussion regarding the luminescence dating results.

Finally, our manuscript benefited from pertinent comments from two anonymous reviewers and those of C. Murray-Wallace. We are grateful to them all.

Appendix 1. Supplementary information

Supplementary material can be found, in the online version, at doi:10.1016/j.quascirev.2009.05.021.

References

Aitken, M.J., Clark, P.A., Gaffney, C.F., 1985. Beta and gamma gradients. Nuclear Tracks and Radiation Measurements 10, 647–653.

Bard, E., 1998. Geophysical and geochemical implications of the radiocarbon calibration. Geochemica et Cosmochemica Acta 62 (12), 2025–2038.

Botter-Jensen, L., 1997. Luminescence techniques: instrumentation and methods. Radiation Measurements 27, 749–768.

Botter-Jensen, L., Mejdahl, V., Murray, A.S., 1999. New light on OSL. Quaternary Science Reviews 18, 303–309.

Botter-Jensen, L., Bulur, E., Duller, G.A.T., Murray, A.S., 2000. Advances in luminescence instrument systems. Radiation Measurements 32, 523–528.

Bowler, J.W., Kotsonis, A., Lawrence, C.R., 2007. Environmental evolution of the Mallee region, Western Murray Basin. Proceedings of the Royal Society of Victoria 118 (2), 161–210.

Coedo, A.G., Padilla, I., Dorado, M.T., 2005. Determination of minor elements in steelmaking flue dusts using laser ablation inductively coupled plasma mass spectrometry. Talanta 67, 136–143.

Duller, G.A.T., 2008. Single grain optical dating of Quaternary sediments: why aliquots size matters in luminescence dating. Boreas 37, 589–612.

Fallon, S.J., Fifield, L.K., Chappell, J.M., The next chapter in radiocarbon dating at the Australian National University: status report on the single stage AMS. Nuclear Instruments and Methods B, in press.

Forbes, M.S., Bestland, E.A., 2006. Guano-derived deposits within the sandy cave fills of Naracoorte, South Australia. Alcheringa Special Issue 1, 129–146.

Forbes, M.S., Bestland, E.A., 2007. Origin of the sedimentary deposits of the Naracoorte Caves, South Australia. Geomorphology 86, 369–392.

Forbes, M.S., Bestland, E.A., Wells, R.T., Krull, E.S., 2007. Palaeoenvironmental reconstruction of the Late Pleistocene to Early Holocene Robertson Cave sedimentary deposit, Naracoorte, South Australia. Australian Journal of Earth Sciences 54, 541–559.

Galbraith, R.F., Roberts, R.G., Laslett, G.M., Yoshida, H., Olley, J.M., 1999. Optical dating of single and multiple grains of quartz from Jinmium rock shelter, northern Australia. Part 1, experimental design and statistical models. Archaeometry 41, 339–364.

Gingele, F.X., De Deckker, P., 2004. Fingerprinting Australia's rivers with clay minerals and the application for the marine record of climate change. Australian Journal of Earth Sciences 51 (3), 339–348.

Gingele, F.X., De Deckker, P., 2005. Clay mineral, geochemical and Sr-Nd isotopic fingerprinting of sediments in the Murray-Darling fluvial system, southeast Australia. Australian Journal of Earth Sciences 52, 965–974.

Harle, K.J., 1997. Late Quaternary vegetation and climate change in southeastern Australia: palynological evidence from marine core E55-6. Palaeogeography, Palaeoclimatology, Palaeoecology 131, 465–483.

Hamilton-Smith, E., 1998. Much ado about very little: bat (*Minioptems schreibersii*) guano mining at Naracoorte, South Australia. Australian Zoologist 30 (4), 387–391.

Huntley, D.J., Hutton, J.T., Prescott, J.R., 1993. The stranded beach-dune sequence of southeast South Australia: a test of thermoluminescence dating 0–800 ka. Quaternary Science Reviews 12, 1–20.

Jacobs, Z., Duller, G.A.T., Wintle, A.G., Henshilwood, C.S., 2006. Extending the chronology of deposits at Blombos Cave, South Africa, back to 140 ka using optical dating of single and multiple grains of quartz. Journal of Human Evolution 51 (3), 255–273.

Laslett, T., 2006. A palaeoecological study of a Quaternary vertebrate fossil deposit in Blanche Cave, Naracoorte, South Australia. Unpublished BSc(Hons) Thesis, Flinders University of South Australia.

Mee, A.C., Bestland, E.A., Spooner, N.A., 2004. Age and origin of terra rossa soils in the Coonawarra area of South Australia. Geomorphology 58, 1–25.

McLennan, S.M., 1989. Rare earth elements in sedimentary rocks: influence of provenance and sedimentary processes. Reviews in Mineralogy and Geochemistry 21, 169–200.

Moriarty, K.C., McCulloch, M.T., Wells, R.T., McDowell, M.C., 2000. Mid-Pleistocene cave fills, megafaunal remains and climate change at Naracoorte, South Australia: towards a predictive model using U-Th dating of speleothems. Palaeogeography, Palaeoclimatology, Palaeoecology 159, 113–143.

Murray, A.S., Wintle, A.G., 2000. Luminescence dating of quartz using an improved single-aliquot regenerative-dose protocol. Radiation Measurements 32, 57–73.

Olley, J.M., Caitcheon, G.G., Murray, A.S., 1998. The distribution of apparent dose as determined by optically stimulated luminescence in small aliquots of fluvial quartz: implications for dating young sediments. Quaternary Geochronology 17, 1033–1040.

Pichevin, L., Cremer, M., Giraudeau, J., Bertrand, P., 2005. A 190 ka record of lithogenic grain-size on the Namibian slope: forging a tight link between past wind-strength and coastal upwelling dynamics. Marine Geology 218, 81–96.

Porat, N., Rosen, S.A., Boaretto, E., Avni, Y., 2006. Dating the Ramat Saharonim Late Neolithic desert cult site. Journal of Archaeological Science 33 (10), 1341–1355.

Prescott, J.R., Hutton, J.T., 1994. Cosmic ray contributions to dose rates for luminescence and ESR dating: large depths and long term variations. Radiation Measurements 23, 497–500.

Prideaux, G.J., Long, J.A., Ayliffe, L.K., Hellstrom, J.C., Pillans, B., Boles, W.E., Hutchinson, M.N., Roberts, R.G., Cupper, M.L., Arnold, L.J., Devine, P.D., Warburton, N.M., 2007. An arid-adapted middle Pleistocene vertebrate fauna from south-central Australia. Nature 445, 422–425.

Reed, E.H., Bourne, S.J., 2000. Pleistocene fossil vertebrate sites of the South East region of South Australia. Transactions of the Royal Society of South Australia 124, 61–90.

Reimer, P.J., Baillie, M.G.L., Bard, E., Bayliss, A., Beck, J.W., Bertrand, C., Blackwell, P.G., Buck, C.E., Burr, G., Cutler, K.B., Damon, P.E., Edwards, R.L., Fairbanks, R.G., Friedrich, M., Guilderson, T.P., Hughen, K.A., Kromer, B., McCormac, F.G., Manning, S., Bronk Ramsey, C., Reimer, R.W., Remmele, S., Southon, J.R., Stuiver, M., Talamo, S., Taylor, F.W., van der Plicht, J., Weyhenmeyer, C.E., 2004. IntCal04 terrestrial radiocarbon age calibration, 0-26 cal kyr BP. Radiocarbon 46, 1029–1058.

Rhodes, E.J., 2007. Quartz single grain OSL sensitivity distributions: implications for multiple grain single aliquot dating. Geochronometria 26, 19–29.

Sprigg, R.C., 1979. Stranded and submerged sea-beach systems of southeast South Australia and the aeolian desert cycle. Sedimentary Geology 22, 53–96.

St Pierre, E., Zhao, J., Reed, E., 2009. Expanding the utility of Uranium-series dating of speleothems for archaeological and palaeontological applications. Journal of Archaelogical Science 36 (7), 1416–1423.

Stuiver, M., Polach, H.A., 1977. Discussion: reporting of ^{14}C data. Radiocarbon 19, 355–363.

Stuiver, M., Reimer, P.J., 1993. Extended 14 C data base and revised CALIB 3.0 14 C age calibration program. Radiocarbon 35, 215–230.

Turner, S., Foden, J., Sandiford, M., Bruce, D., 1993. Sm-Nd isotopic evidence for the provenance of sediments from the Adelaide Fold Belt and southeastern Australia with implications for episodic crustal addition. Geochimica et Cosmochimica Acta 57 (8), 1837–1856.

Wells, R.T., Moriarty, K., Williams, L.G., 1984. The fossil vertebrate deposits of Victoria fossil cave Naracoorte: an introduction to geology and fauna. Australian Zoologist 21 (4), 305–333.